

# **SANDIA REPORT**

SAND2010-4362  
Unlimited Release  
Printed July 2010

## **Transient PVT Measurements and Model Predictions for Vessel Heat Transfer— Part I**

Steven F. Rice, Nicholas J. Paradiso, Todd G. Felver,  
William S. Winters, Gregory H. Evans

Prepared by  
Sandia National Laboratories  
Albuquerque, New Mexico 87185 and Livermore, California 94550

Sandia National Laboratories is a multi-program laboratory managed and operated by Sandia Corporation, a wholly owned subsidiary of Lockheed Martin Corporation, for the U.S. Department of Energy's National Nuclear Security Administration under contract DE-AC04-94AL85000.

Approved for public release; further dissemination unlimited.

Issued by Sandia National Laboratories, operated for the United States Department of Energy by Sandia Corporation.

**NOTICE:** This report was prepared as an account of work sponsored by an agency of the United States Government. Neither the United States Government, nor any agency thereof, nor any of their employees, nor any of their contractors, subcontractors, or their employees, make any warranty, express or implied, or assume any legal liability or responsibility for the accuracy, completeness, or usefulness of any information, apparatus, product, or process disclosed, or represent that its use would not infringe privately owned rights. Reference herein to any specific commercial product, process, or service by trade name, trademark, manufacturer, or otherwise, does not necessarily constitute or imply its endorsement, recommendation, or favoring by the United States Government, any agency thereof, or any of their contractors or subcontractors. The views and opinions expressed herein do not necessarily state or reflect those of the United States Government, any agency thereof, or any of their contractors.

Printed in the United States of America. This report has been reproduced directly from the best available copy.

Available to DOE and DOE contractors from

U.S. Department of Energy  
Office of Scientific and Technical Information  
P.O. Box 62  
Oak Ridge, TN 37831

Telephone: (865) 576-8401  
Facsimile: (865) 576-5728  
E-Mail: [reports@adonis.osti.gov](mailto:reports@adonis.osti.gov)  
Online ordering: <http://www.osti.gov/bridge>

Available to the public from

U.S. Department of Commerce  
National Technical Information Service  
5285 Port Royal Rd.  
Springfield, VA 22161

Telephone: (800) 553-6847  
Facsimile: (703) 605-6900  
E-Mail: [orders@ntis.fedworld.gov](mailto:orders@ntis.fedworld.gov)  
Online order: <http://www.ntis.gov/help/ordermethods.asp?loc=7-4-0#online>



# Comparison of High Pressure Transient PVT Measurements and Model Predictions – Part I

Steven F. Rice, Nicholas J. Paradiso, Todd G. Felver  
Gas Transfer Systems

William S. Winters, Gregory H. Evans  
Thermal/Fluid Science and Engineering

Sandia National Laboratories  
P.O. Box 969  
Livermore, CA 94550

## Abstract

A series of experiments consisting of vessel-to-vessel transfers of pressurized gas using Transient PVT methodology have been conducted to provide a data set for optimizing heat transfer correlations in high pressure flow systems. In rapid expansions such as these, the heat transfer conditions are neither adiabatic nor isothermal. Compressible flow tools exist, such as NETFLOW that can accurately calculate the pressure and other dynamical mechanical properties of such a system as a function of time. However to properly evaluate the mass that has transferred as a function of time these computational tools rely on heat transfer correlations that must be confirmed experimentally. In this work new data sets using helium gas are used to evaluate the accuracy of these correlations for receiver vessel sizes ranging from 0.090 L to 13 L and initial supply pressures ranging from 2 MPa to 40 MPa. The comparisons show that the correlations developed in the 1980s from sparse data sets perform well for the supply vessels but are not accurate for the receivers, particularly at early time during the transfers. This report focuses on the experiments used to obtain high quality data sets that can be used to validate computational models. Part II of this report discusses how these data were used to gain insight into the physics of gas transfer and to improve vessel heat transfer correlations. Network flow modeling and CFD modeling is also discussed.

## **ACKNOWLEDGMENTS**

The authors would like to thank Cindy Alvine, Tim Sage, Dan Yee, and Annette Newman for technical support on test vessel qualification and experimental support.

# CONTENTS

1. Introduction.....	9
2. Experimental method.....	11
2.1. Apparatus.....	11
2.1.1. Vessels.....	12
2.1.2. Valve.....	14
2.1.3. High pressure supply.....	14
2.1.4. Instrumentation.....	14
2.1.5. Volumes.....	14
2.2. Methods.....	15
2.2.1. Procedures.....	15
2.2.2. Data reduction – calculating $T_{avg}$ .....	19
3. Experimental Results.....	23
3.1. 13L receiver.....	23
3.1.1. General characteristics.....	23
3.1.2. Error analysis.....	26
3.2. 700 cc receiver.....	27
3.2.1. General characteristics.....	27
3.2.2. Mass balance.....	28
3.3. 90 cc receiver.....	29
3.3.1. General characteristics.....	29
3.3.2. Mass balance.....	30
4. Comparison with Netflow.....	31
4.1 Heat transfer correlations.....	31
4.2 Model-data comparisons.....	34
4.3 Modeling summary.....	39
5. Conclusion.....	41
6. References.....	43
Distribution.....	45

## FIGURES

Figure 1. Schematic of 200 cc - 700 cc vessel configuration .....	11
Figure 2. Photograph of vessel configuration 200 - 700 cc .....	12
Figure 3. Hemispheres for the 700 cc vessel .....	12
Figure 4. From left, 90 cc, 200 cc, 600 cc (not used), and 700cc vessels.....	13
Figure 5. a) 200 cc supply configured with 13L receiver b) 13L vessel .....	13
Figure 6. Details of test volumes for the 200-700 300 psi blowdown.....	15
Figure 7. Receiver flow delays .....	17
Figure 8. Supply flow delays .....	18
Figure 9. TPVT record showing continued flow out of the supply into the tubing downstream of the orifice after the ball valve has fully closed .....	18
Figure 10. Pressure behavior of the supply and receiver vessels with the closure valve functioned at 1.02 s.....	19
Figure 11. Supply and receiver pressures for flow into the 13L receiver.....	23
Figure 12. 13L receiver thermocouples (Tc) and TPVT Tav <sub>g</sub> from 6000 psi supply .....	24
Figure 13. Supply thermocouples and Tav <sub>g</sub> .....	24
Figure 14. 13L receiver and supply pressures .....	25
Figure 15. Supply thermocouples and TPVT Tav <sub>g</sub> .....	26
Figure 16. Mass balance for the 6000 psia blowdown into the 13000 cc vessel .....	27
Figure 17. Pressure traces for the 3000 psi blowdown into the 700cc receiver.....	27
Figure 18. TPVT Tav <sub>g</sub> for the 3000 psi 700 cc receiver blowdown .....	28
Figure 19. Mass balances error for the three 700 cc receiver experiments.....	28
Figure 20. Pressure records for the 6000 psi blowdown into the 90 cc receiver .....	29
Figure 21. Comparison of the TPVT Tav <sub>g</sub> temperatures and the internal thermocouples for the 6000 psi blowdown into the 90 cc receiver .....	30
Figure 22. 90 cc receiver mass error.....	30
Figure 23. Measured and predicted supply (200 cc) and receiver (700 cc) mass averaged temperatures. Initial supply pressure was 300 psi (nominal).....	35
Figure 24. Measured and predicted supply (200 cc) and receiver (700 cc) mass averaged temperatures. Initial supply pressure was 3000 psi (nominal).....	35
Figure 25. Measured and predicted supply (200 cc) and receiver (700 cc) mass averaged temperatures. Initial supply pressure was 6000 psi (nominal).....	36
Figure 26. Measured and predicted supply (200 cc) and receiver (90 cc) mass averaged temperatures. Initial supply pressure was 3000 psi (nominal).....	37
Figure 27. Measured and predicted supply (200 cc) and receiver (90 cc) mass averaged temperatures. Initial supply pressure was 6000 psi (nominal).....	37
Figure 28. Measured and predicted supply (200 cc) and receiver (13 liter) mass averaged temperatures. Initial supply pressure was 6000 psi (nominal).....	38
Figure 29. Measured and predicted supply (200 cc) and receiver (13 liter) mass averaged temperatures. Initial supply and receiver pressures: 360 and 200 psia respectively ..	39

## TABLES

Table 1. Experimental Volumes .....	16
Table 2. Helium Compressibility Coefficients $k_{i,j}$ .....	21



# 1. INTRODUCTION

The rapid flow of gas from one pressurized vessel to another, the associated pressure changes, and in particular transfer of mass is at the heart of the GTS mission. Since the mid 1970's, there has been effort directed at modeling the compressible flow in vessels and tubes in order to improve system design as well as for other analytical purposes associated with GTS surveillance observations and QMU assessment.

The nature of these rapid transfers is such that the conditions over the time period of the transfer event are neither adiabatic nor isothermal. As a result, compressible flow models of these events need to account for heat transfer between the pressure vessel and the gas. Inaccurate modeling of heat transfer will effect predictions for the net mass transferred as a function of time.

This particular fluid flow and heat transfer topic dates back over 250 years. The history and literature is well documented by Johnston [1] and is discussed extensively in Part II of this report. In Johnston's work, Transient PVT (TPVT) measurements were carefully evaluated with particular attention to flow instabilities for relatively low pressure gas sources. This work was followed by other experimental work not well documented leading to the development of a simple compressible flow computational model, TRIC, developed by Clark in the early 1980s [2]. In TRIC, heat transfer correlations derived by Means [3,4] and later modified by Meyer [5] are implemented (see Clark [2] for documentation). The origin of these adjustments to the Means expressions or the data from which these adjustments are derived appears undocumented. The comparison of the TRIC results to the TPVT measurements of Libkind are reported in Clark [2]. That analysis refers to six transfers using a 201 cc supply vessel and a 14700 cc receiver but only shows results from two supply and one receiver experiment. The interpretation of the receiver record is complicated as it originates from functioning the system in reverse with the 201 cc vessel serving as the receiver. Clark concludes that the source heat transfer correlation in TRIC is sound showing two sets of data where source vessel pressures and average temperatures are well represented by TRIC calculations when using the Meyer heat transfer parameters. The results for the receiver are less conclusive with the data for one experiment showing moderately good comparison with the calculations when the heat transfer model was again modified for the "active" part of the fill.

Since the development of TRIC, Winters developed TOPAZ [6-10] followed by NETFLOW [11] and compared the most recent version of NETFLOW with the Libkind results and some preliminary results associated with the work presented in this report [12].

This report presents the experimental details of seven TPVT experiments from a single source vessel into three receivers varying in volume over a factor of 100. Helium gas was used exclusively. The flow configuration is described in detail along with the data reduction methods. The TPVT data are reduced to solve for an average temperature of the gas in both supply and receiver vessels as a function of time throughout the transfer process.

This report establishes two aspects of the dual vessel flow modeling using NETFLOW that had as yet not been fully explored. First, the data and model comparison provide for validation of the source heat transfer correlation over a range of source pressures from 300 to 6000 psi. Second this report shows in a much clearer way that the receiver heat transfer correlations are indeed poor. In order to ultimately develop a model of the overall process of compressible choked flow from one vessel to another, more work will be required to properly describe the receiver characteristics. The development of new CFD models for gas transfer is discussed extensively in Part II of this report.

These data also support a follow on effort to establish the ability to directly calculate the heat transfer by way of a compressible flow 3-D Navier Stokes approach. The Sandia flow and heat transfer code, FUEGO, has undergone some modifications to attempt this task. It is hoped that, when completed, these data supply a useful start for the validation of the constitutive models contained within.

## 2. EXPERIMENTAL METHOD

The experiments consisted of conducting measurements on the transfer of gas from one vessel to another using the well-established TPVT method. The method is described in detail by Johnston [1] and others. The key to the method is to directly measure the amount of mass that has either left a supply vessel or entered a receiver over the course of time during the transfer. This can be done by abruptly stopping the flow at a number of different times during repeated identical transfers and then permitting the entire system to return to thermal and pressure equilibrium. Using suitable pressure and temperature measurement sensors along with an appropriate equation of state, the total mass in both the supply and the receiver can be calculated. By repeating a series of identical measurements varying only in the time the flow is stopped, the true mass transfer profile can be obtained. These mass transfer data can be compared with the transient vessel pressures measured at the point in time of valve closure to arrive at an average temperature for the gas in either vessel,  $T_{avg}$ .

### 2.1. Apparatus

The experimental apparatus consisted of a single supply volume and three interchangeable receiver volumes. The supply was nominally 200 cc in volume and the three receivers were nominally 13000 cc, 700 cc, and 90 cc. In all configurations, the supply and receiver were connected by several small lengths of tubing and a fast acting solenoid driven ball valve. Figure 1 shows an illustration of the configuration with the 700 cc receiver. Figure 2 shows a photograph of the assembly. The supply and receiver vessels and the flow path connecting them were deliberately configured in a vertical orientation in order to facilitate axisymmetric modeling of the experiment using CFD code. The predominant flow loss in the path between the supply and the receiver was a 0.020 inch diameter orifice located at the supply exit.

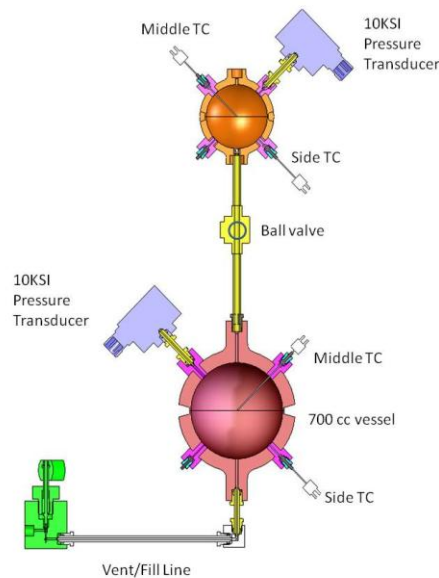


Figure 1. Schematic of 200 cc - 700 cc vessel configuration



**Figure 2. Photograph of vessel configuration 200 - 700 cc**

### **2.1.1. Vessels**

Three thick walled high pressure vessels were fabricated from 21-6-9 stainless steel and qualified for manned-use at pressures over 70 MPa. The vessels were constructed from two hemispheres and joined using a multipass IGTA weld. The vessels were equipped with a number of ports to provide access for pressure transducers as well as fill and vent tubes. The two hemispheres used to construct the 700 cc vessel are shown in Figure 3. Figure 4 shows a photograph of four vessels with nominal volumes: 90 cc, 200cc, 600 cc (not used), and 700 cc.



**Figure 3. Hemispheres for the 700 cc vessel**



**Figure 4. From left, 90 cc, 200 cc, 600 cc (not used), and 700cc vessels**

The 13 L vessel is a sphere that was also assembled from two stainless steel hemispheres (~ 0.5 inch thick) and is equipped with a number of access ports with standard pressure fittings. Figure 5 shows the 13L vessel in the test configuration and a photograph of the vessel alone.

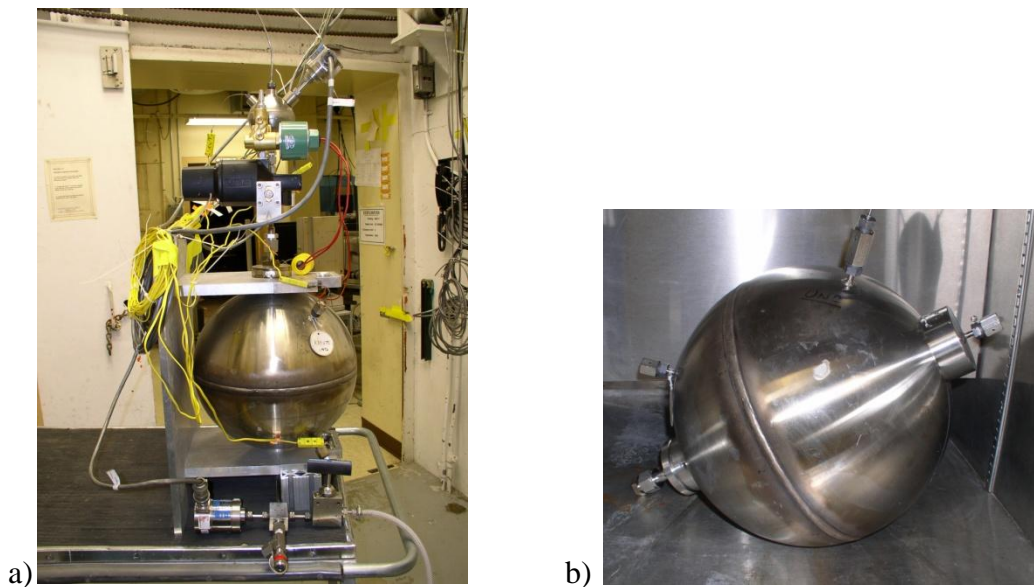


**Figure 5. a) 200 cc supply configured with 13L receiver b) 13L vessel**

The volumes of all four vessels were determined using Sandia's precision volume measurement apparatus. The reported vessel volumes in Table 1 are accurate to  $\pm 0.04\%$  [13].

The 200 cc supply vessel remained essentially in the same configuration for all experiments. The 200 cc vessel is similar to the 700 cc and 90 cc high pressure receiver vessels with the exception that within the outlet port there is a 0.020 inch diameter orifice. As previously mentioned, the orifice functions to limit the flow rate such that the entire pressure drop in the flow occurs at this point and that any additional flow restriction originating from the tubing between the two vessels is negligible. This was done to simplify the modeling of the flow path connecting the vessels.

### *2.1.2. Valve*

The solenoid-actuated valve at the center of the experiment is a ¼ turn ball valve with a 0.5 in diameter (ball size). The valve functions from a fully closed to a fully open state in 0.054 s (full quarter- turn). The reversed closure time is 0.30 s. The times between when valve is fully open and fully closed are recorded by having an extension of the valve arm make contact with switches at both the fully open and fully closed extremes. Both actions show several milliseconds jitter around these values. However, the time required to establish steady flow is much shorter as that is the time for the cross sectional area of the flow passage in the ball to overlap and become sufficiently aligned with the inlet and outlet holes such that the primary source of restriction in the flow sources from the 0.020 in orifice in the supply vessel. The valve only needs to be open with a cross sectional area that is greater than about 0.005 cm<sup>2</sup> (approximately 2.5X the orifice area). Geometrical analysis reveals that given a 0.050 s full swing for ¼-turn of the valve, a 0.005 cm<sup>2</sup> passage occurs in about 2 ms, assuming the valve angular rotation rate is linear in time. The time resolution of the data acquisition was typically 1 ms/point and therefore the valve can be considered to open and close nearly instantaneously and will not be considered a factor in the subsequent analysis. Thus the overall time resolution of the experiment is on the order of a few milliseconds.

### *2.1.3. High pressure supply*

All experiments were conducted using helium gas provided within the Building 966 gas system. A Hydropac compressor was used to fill the vessels for the 6000 psi and 3000 psi fill conditions.

### *2.1.4. Instrumentation*

All data were recorded on Nicolet Odyssey data recorder. Pressures were measured using Teledyne Taber dynamic pressure transducers (varying Model #'s and ranges) and temperatures were measured using Omega 0.030 in Type K sheathed grounded thermocouples. The calibration of the data recorders and pressure transducers is maintained in Building 966 calibration program. The thermocouples were installed new and used “as is”. Over the course of the experimental campaign a number of different pressure transducers were used to best cover the range of pressures observed during the blow down.

### *2.1.5. Volumes*

Because the different experiments were conducted over a broad pressure range slightly different configurations were required and the cumulative supply and receiver volumes varied slightly. Figure 6 show a detail schematic of the various connections and Table 1 lists all of the volumes for the seven experiments addressed in this report.

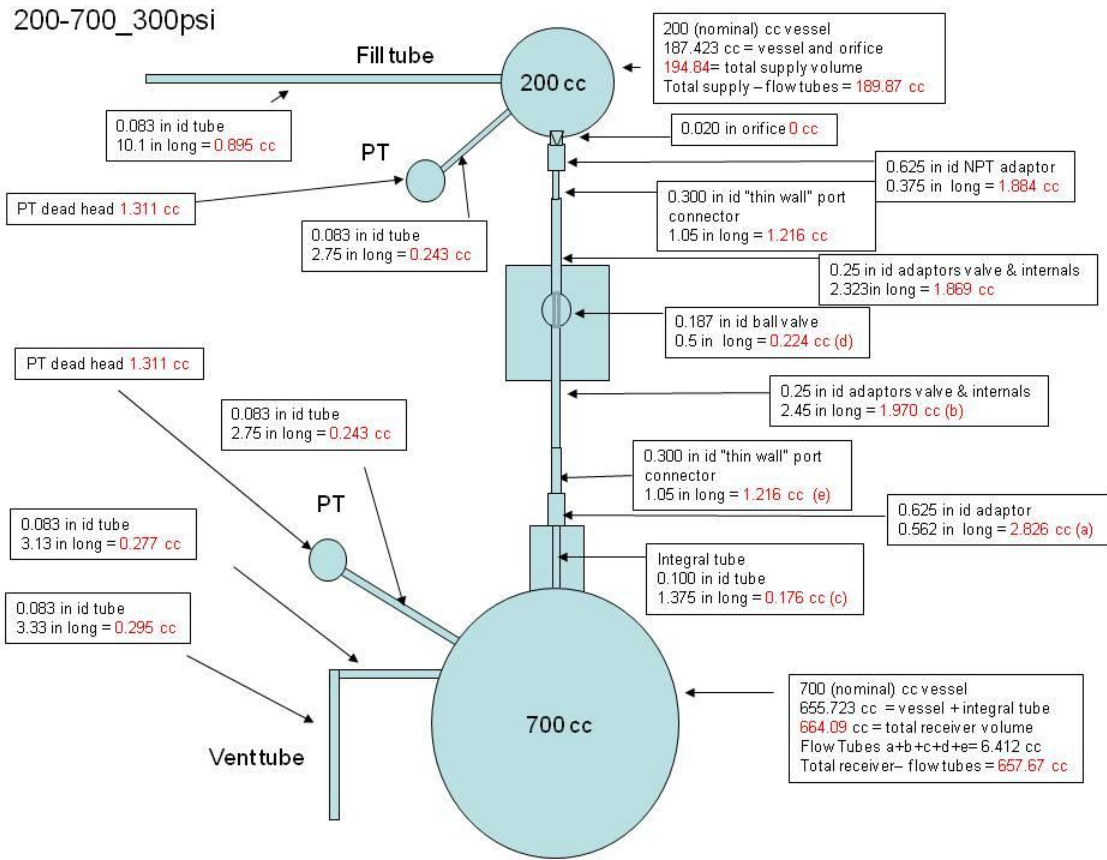


Figure 6. Details of test volumes for the 200-700 300 psi blowdown

## 2.2. Methods

### 2.2.1. Procedures

The experiments were conducted as a series of transfers all with the same starting conditions but with different predetermined times that the transfer valve was closed. Typical data sets recorded transfers of 0.1 s to 30 s. Each time step recorded pressure in both vessels, center and near side wall temperatures in both vessel and timing fiducials when the valve arrived at the fully open or fully closed position described above. Each closure time data set was recorded with 0.001 s time resolution for a duration of 60 s to reach thermal equilibrium with the exception of the 13L receiver data which used a 0.01 s timestep.

The primary measurements taken are the initial, dynamic, and final pressures in the vessels, as well as initial and final vessel temperatures. With these measurements the amount of transferred mass at any given stopped flow time can be determined. The transient mass transferred is determined from the final pressure and temperature after permitting the pressure and temperature to equilibrate. This equilibration time was about 40 s for the smaller receiver and closer to 60s for the 13000 cc receiver.

**Table 1. Experimental Volumes**

<b>part</b>	<b>300-13K 6000psi<sup>a</sup></b>	<b>200-700 300 psi</b>	<b>200-700 3000 psi</b>	<b>200-700 6000 psi</b>	<b>200-90 3000 psi</b>	<b>200-90 6000 psi</b>
supply	187.423	187.423	187.423	187.423	187.423	187.423
supply fill tube	0.895	0.895	0.895	0.895	0.895	0.895
supply PT tube	0.243	0.243	0.243	0.243	0.243	0.243
Supply PT	1.987	1.311	1.147	1.967	1.147	1.967
supply adaptor	1.884	1.884	1.884	1.884	1.884	1.884
supply port connector	1.216	1.216	1.216	0.844	0.844	0.844
supply flow tube	1.869	1.869	1.869	1.869	1.869	1.869
receiver	12909.599	655.723	655.723	655.723	81.173	81.173
rec PT tube	0.243	0.243	0.243	0.243	0.243	0.243
rec PT	1.311	1.311	1.311	1.311	1.311	1.147
receiver vent tube 1	0.51	0.277	0.277	0.277	0.277	0.277
receiver vet tube 2	0.52	0.295	0.295	0.295	0.295	0.295
rec adaptor	2.826	2.826	2.826	2.826	2.826	2.826
rec port connector	1.216	1.216	1.216	1.216	0.844	0.844
rec integral tube	3.6	0.176	0.176	0.176	0.125	0.125
rec flow tube	1.970	1.970	1.970	1.970	1.970	1.970
ball valve	0.224	0.224	0.224	0.224	0.224	0.224
relief device	0.8	0	0	0	0	0
supply total volume	195.52	194.84	194.68	195.13	194.31	195.13
supply volume w/o flow tubes	190.55	189.87	189.71	190.53	189.71	190.53
flow tube	4.97	4.97	4.97	4.60	4.60	4.60
receiver total volume	12919.22	664.09	664.09	664.09	89.16	89.00
receiver vol. w/o flow tubes	12908.58	657.67	657.67	657.67	83.17	83.01
flowtube	10.64	6.41	6.41	6.41	5.99	5.99

a-The volume for the pressure transducers are not certain in the 360 -200 psi 13L. The overall volumes are near that of the 6000 psi experiment.

b-Volumes in RED are values that change from preceding column

The other important measurement is the open and closure time of the valve, since the precise position of the valve is not known during the opening and closing turns. However, it is easy to use the actual data itself to determine these times. Figure 7 shows typical pressure traces for the receiver pressure in the vicinity of the initial valve opening and valve closure along with a trace from a full blowdown when there is no transient valve closure. Figure 8 shows a similar plot for

the supply. Upon valve opening, it can be seen that there is approximately an 18 -21 ms delay from initial valve movement, indicated by the switch signal, until gas starts to flow and a pressure rise is observed on the receiver as well as a corresponding drop on the supply. Figure 7 also shows that on closure there is an 8 ms delay between the end of the pressure rise and full closure of the valve indicated by the closure switch dropping to zero volts. These two points, accurate to about 2-3 ms are used to determine the duration of the flow. The transient flow duration for the receiver is determined by using these observations marking initiation and cessation of flow.

Because of the experimental configuration there are additional considerations required to obtain the supply transient close pressure. The supply side of the valve has two important volumes: 1) the vessel itself (plus small volumes due to the fill tubes and pressure transducer connectors dead head volume); and 2) the 4.6 cm<sup>3</sup> tubing volume between the supply orifice and the ball valve. This additional volume complicates the analysis of the flow in two ways.

- 1) Before the valve is opened, there is about 2% of the supply gas already past the orifice and this gas flows into the receiver very quickly upon opening (see Figure 7). This is not an especially significant problem since the data analysis method used to obtain the receiver  $T_{avg}$  is not affected by change in flow rate. That is, the transient pressure is still accurate and the final pressure and temperatures are unaffected.
- 2) When the valve closes, the supply vessel upstream of the orifice and the 4.6 cm<sup>3</sup> of tubing downstream are not in pressure equilibrium. To rephrase, for TPVT experiments with stop times faster than about 1.5 s, the supply and the tubing volume are not at the same pressure at the instant of valve closure because the pressure drop occurs at the orifice. Gas continues to flow into the 4.6 cm<sup>3</sup> transfer tube volume until the pressures are equal across the orifice. For the earliest time measurements, this is as much as 30 ms. Figure 9 show this for a TPVT datum taken at 0.114 s. . This presents a problem in determining the appropriate time assigned as “valve close” from the standpoint of evaluating the transient supply pressure at closure.

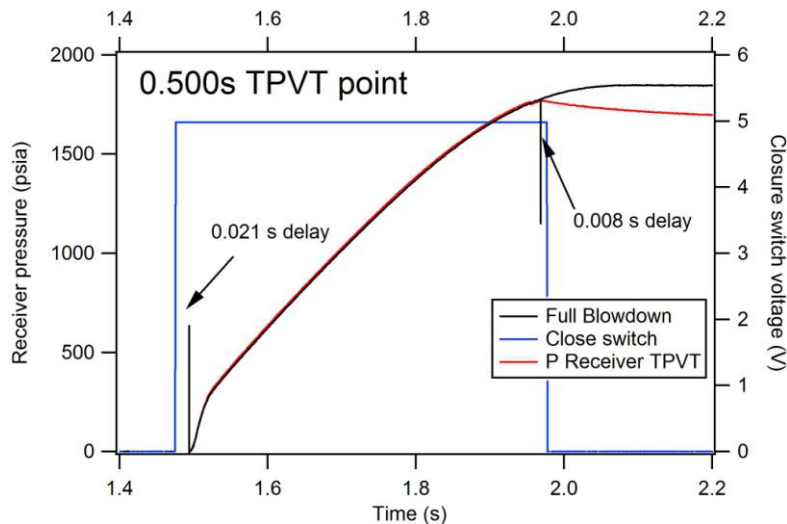


**Figure 7. Receiver flow delays**

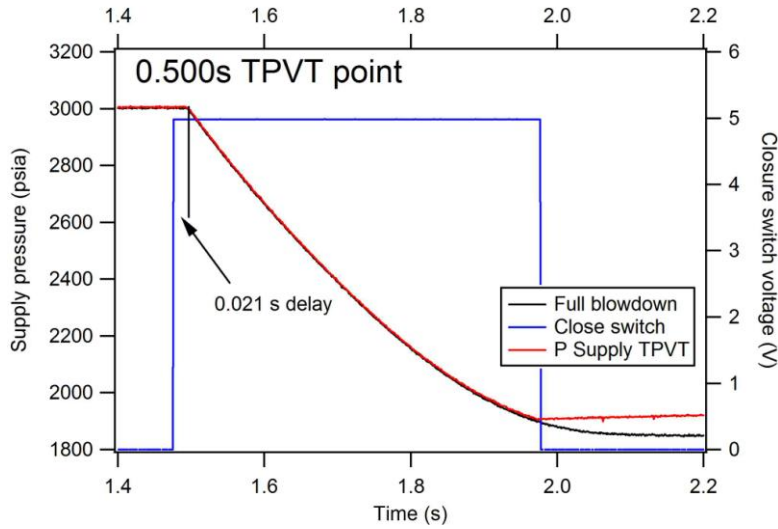


**Figure 8. Supply flow delays**

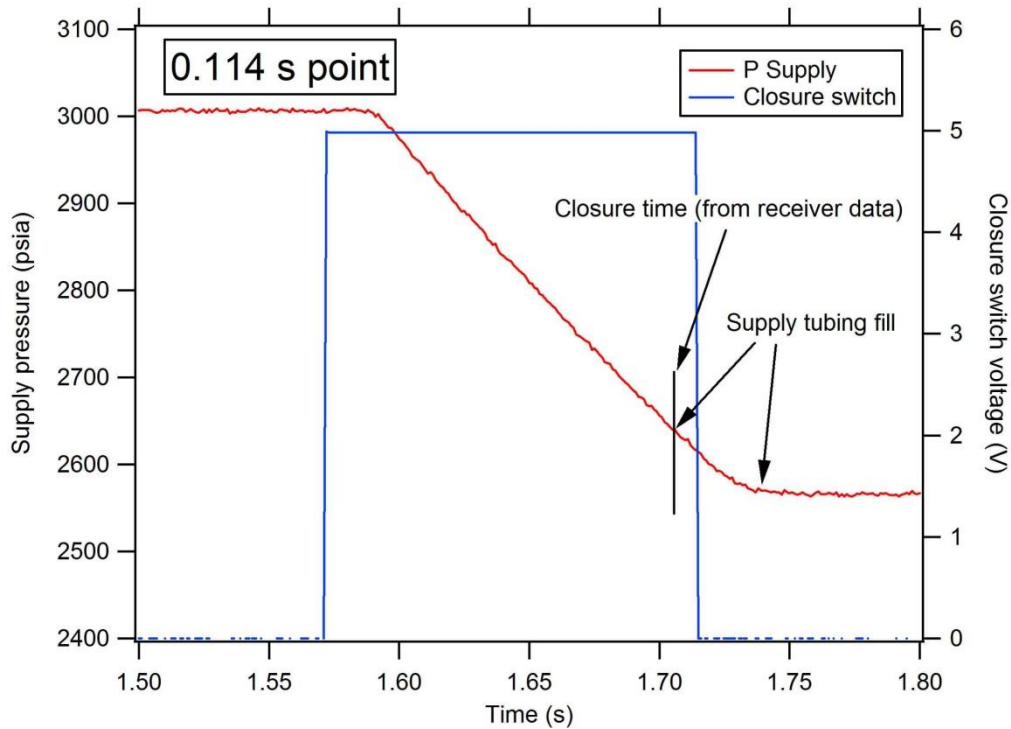


**Figure 9. TPVT record showing continued flow out of the supply into the tubing downstream of the orifice after the ball valve has fully closed**

For the purposes of the analysis used to determine the supply closure time and the transient pressure, the “close” time and “close” pressure are taken to be when the supply tubing and supply vessel have reached equilibrium. Again, similar to the early rapid filling of the receiver, this does not affect the accuracy of the value obtained for the true mass transfer rate as a function of time. However, it does effect the evaluation of the transient  $T_{avg}$  in the supply vessel. This

approach provides a much more accurate value for the transient  $T_{avg}$  in the supply since it is a proper evaluation of the  $P_{avg}$  of the combined two sides of the orifice at closure. Error is introduced only by way of the heat that is transferred within the supply during these few dozen milliseconds. As can be seen for the data below, the supply heat transfer rate, even at the extreme in the transfer corresponds to less than 1 °C in 20 ms.

If this approach is not taken, and the pressure at closure is taken as the pressure indicated by the supply transducer at valve closure time, the calculated  $T_{avg}$  for early times will appear as a physically meaningless *increase* in temperature as the transient  $P_{close}$  will be actually higher than the equilibrated  $P_{final}$ .

For illustration purposes, Figure 10 shows the pressure behavior of a typical TPVT data point. The records in the figure are taken for a 1.02 s TPVT test. The figure shows the recovery time of about 30 s from the valve closure to thermal equilibration for both the supply and receiver.

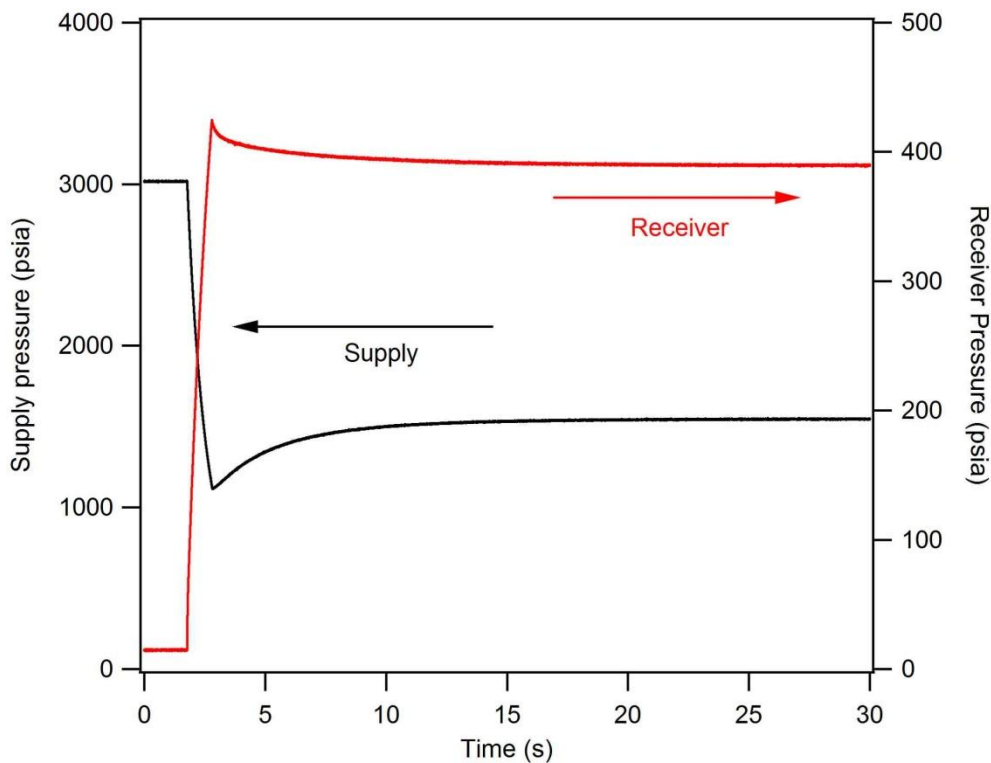


**Figure 10. Pressure behavior of the supply and receiver vessels with the closure valve functioned at 1.02 s**

### 2.2.2. Data reduction – calculating $T_{avg}$

$T_{avg}$  is calculated by evaluating the amount of mass transferred at a given time of valve closure by permitting both vessels to equilibrate and then evaluating a non-ideal EOS using  $P_{final}$  and  $T_{final}$  and the vessel volume. Once the transferred mass is known the same EOS is used to calculate temperature in the vessel at closure using the pressure at closure in the case of the receiver or pressure at flow equilibrium for the supply tubing (discussed above).

The data are recorded as a series of individual expansions as described above in 2.2.2. Each file was digested using a data analysis procedure written in Wavemetrics Inc. IGOR Pro Data analysis application. This procedure automatically determines the time points in the transfers, extracts the transient and equilibrium data, and loads it into a convenient table that can be exported to Excel. The Excel spreadsheet is then used for calculation of  $T_{avg}$  and checking mass balances.

As a number of the experiments are conducted at high pressure a non-ideal EOS is needed to properly evaluate the results. The best available EOS for helium is imbedded in the SNL code FILLUP based on the work of Keeton [14]. However, this EOS is in the explicit form of  $Z_{Fillup}(T, \rho)$  and cannot be algebraically converted to the form needed for this application,  $\rho(P, T)$ , providing the observed final equilibrated ole quantity transferred  $n_f$  from  $P_f$  and  $T_f$ . In order to use the FILLUP EOS an iterative approach is needed.

Procedure:

- 1) Estimate  $\rho_f$  as  $\rho_{AN}$  using the Abel-Noble(AN) non-ideal gas equation of state described

$$\rho_{AN} = \frac{P_f}{RT_f + B_{AN}P_f} \quad (1)$$

where  $B_{AN} = 0.002673 \text{ m}^3/\text{kg}$  for helium.

- 2) The  $\rho_{AN}, T_f$  expansions in the FILLUP polynomials are used to get a  $Z_{Fillup}$ . In principle this new  $Z_{Fillup}$ , when combined with the measured  $P_f$  and  $T_f$  will result in a slightly different  $\rho_{Fillup}$  than that originally calculated using the AN EOS and the procedure could be repeated to closure. As it turns out, only this first iteration is needed even at 6000 psi where the difference between the initial  $\rho_{AN}$  and  $\rho_{Fillup}$  is about 1%. A second iteration is well beyond the data accuracy.

The FILLUP EOS is expressed as an expansion in  $Z_{Fillup}(T, \rho)$

$$b_i = \sum_{j=0,3} k_{ij} T^{j-1} \quad (2)$$

$$Z_{Fillup} = 1 + \rho_{AN} \{ b_0 + \rho_{AN} [ b_1 + \rho_{AN}(b_2 + \rho_{AN}b_3) ] \} \quad (3)$$

followed by solving for a new  $\rho_{Fillup}$ ,

$$\rho_{Fillup} = \frac{P_f}{Z_{Fillup}RT_f} = \frac{n_f}{V} \quad (4)$$

**Table 2. Helium Compressibility Coefficients  $k_{i,j}$**

$j \backslash i$	0	1	2	3
0	-1.115170E+03	2.018512E+04	0	0
1	2.460812E+01	0	0	4.345040E+04
2	-4.409928E-02	2.134515E-01	3.262888E+00	-1.541939E+02
3	4.348201E-50	-3.255642E-04	0	0

- 3)  $T_{avg}$  is then calculated using the AN EOS with the closure pressure and the equilibrated net mass in the vessel obtained in Step 2. Using the Fillup EOS for this step has no measureable advantage since the  $T_{avg}$  calculation is essentially the result from the differences in pressures at closure and equilibration and the error in the EOS at comparable pressures nearly cancel. Any error introduced using this method is well below the error in the data.

$$T_{avg} = \frac{P_f(1 - B_{AN}\rho_{Fillup})}{\rho_{Fillup}RT_f} \quad (5)$$

### 2.2.3. Mass balance

The individual TPVT points were checked for mass balance. In most experiments with the 700 or 90 cc receivers, the deviation for initial mass to final is less than 2%. The accuracy of the overall mass balance is sensitive to the accuracy to which the excess volumes originating from flow tubing and pressure transducer on the supply assembly are known and of course the accuracy of the pressure transducers themselves. Special effort was placed on knowing these volumes accurately.

In all instances where the mass balance deviated by more than 0.3 % the characteristic of the trends all indicate systematic deviation following the behavior of the gas flow. That is, the mass error increased or decreased monotonically with the fraction of gas transferred indicating the source of error is associated with the measurement accuracy of the transducers or the total vessel volume.

The quoted error on the transducers varied to some degree from model to model, but typically the error is listed in three parts: reproducibility (0.15% FS), linearity (0.1% FS), and hysteresis (0.1 % FS). The most conservative approach is to add these three contributions together to arrive at the overall absolute error. Obviously, if a transducer is being used at only a fraction of the full scale (FS) of the sensor range the fractional error on a given measurement could be considerable. This problem is particular acute in the instance of the 200-13000 experiment where the 13000 cc vessel was equipped with a 500 psi transducer. Indeed, the mass balance on the 200-13000 experiment is poorer than the others with an observed maximum deviation of 2.7%.



### 3. EXPERIMENTAL RESULTS

#### 3.1. 13L receiver

These were the first TPVT experiments conducted. The first experiment involved a high pressure expansion from the 200 cc supply that was originally filled to 6000 psi. The second experiment was much different. In that case, the expansion was from a 360 psi 200 cc supply into the 13 L receiver that had already been filled to 200 psi. The experiment was designed to ensure that flow to the receiver was not choked and therefore the supply depressurization would be very well characterized. For both of these experiments the data were collect at 0.010 s interval. After these initial experiments it was realized that higher time resolution was desirable and all the subsequent experiments were conducted with 0.001s timestep.

##### 3.1.1. General characteristics

Figure 11 shows the transient pressures for the full expansion indicating that pressure equilibrium was reached at ~8 s. Figure 12 show the  $T_{avg}$  TPVT results of the receiver plotted along with the thermocouples located at the center and the edge of the vessel. Thermal equilibrium is not quite achieved even though after the full 15 s experimental time the pressure differential is less than 10 psi after 8 s. Figure 13 shows the same data for the supply. The overall mass balance on this experiment was the poorest of all the experiments, with the deviation being as high as 2.75 %.

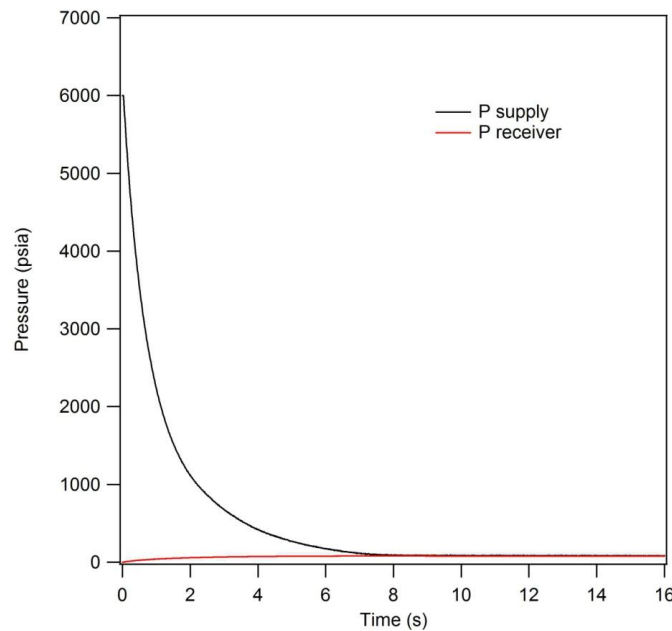


Figure 11. Supply and receiver pressures for flow into the 13L receiver

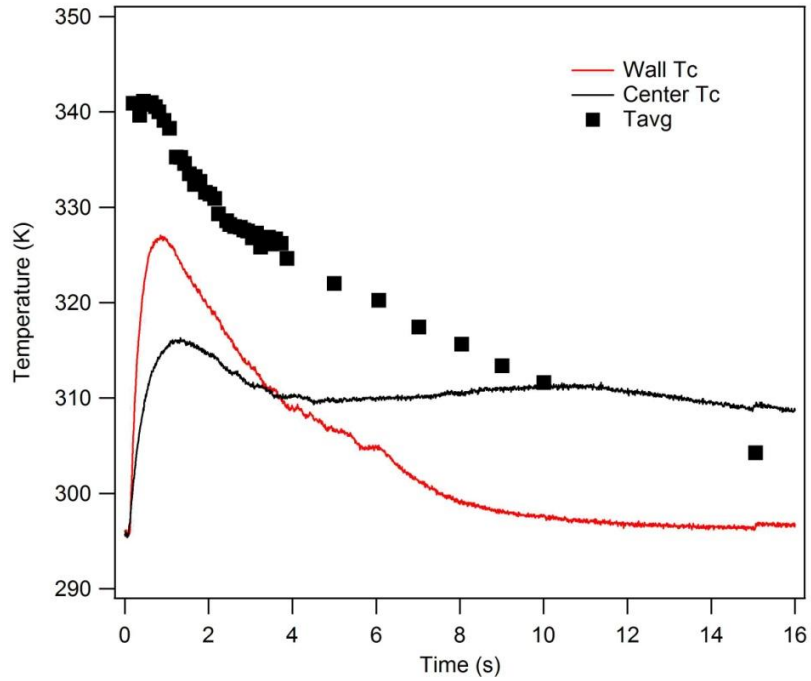


Figure 12. 13L receiver thermocouples (Tc) and TPVT Tavg from 6000 psi supply

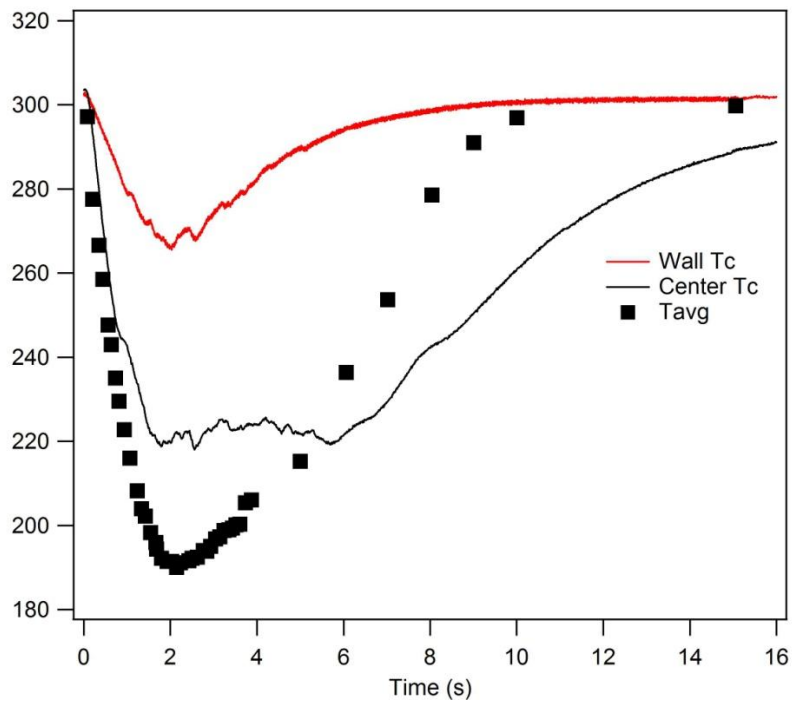
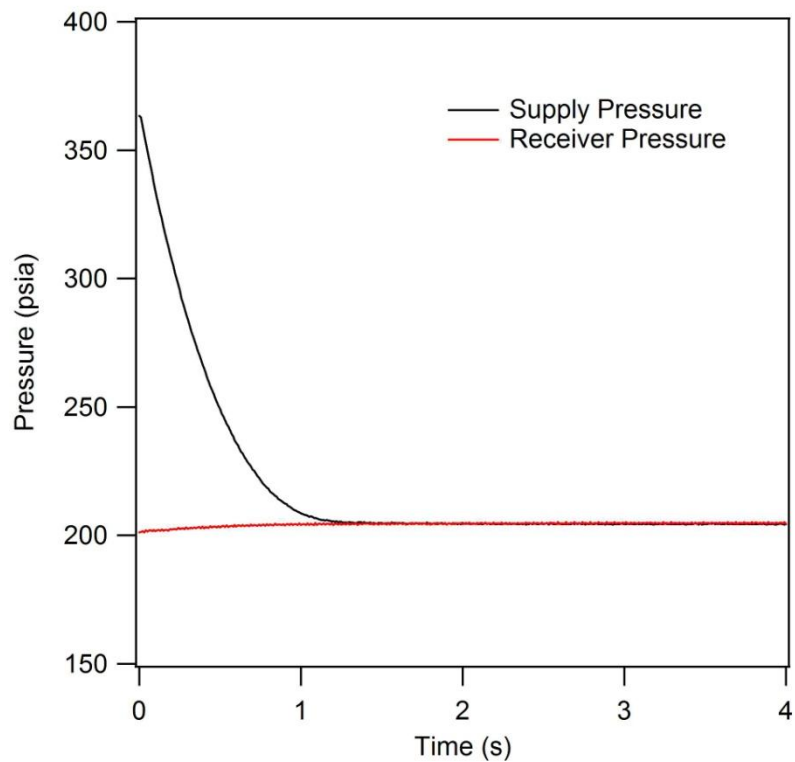


Figure 13. Supply thermocouples and Tavg

Note that the dynamic measurements indicate that neither the center thermocouple nor the side thermocouple reach the  $T_{avg}$  temperature even at maximum excursion and the center Tc is cooler than the side Tc at early time. Note too that the value of  $T_{avg}$  does not lie between the observed near-wall and near center thermocouples. Presumably this is because the center Tc is located directly in the path of the cold jet entering the vessel and that colder fill gas has not yet reached equilibrium with the entire vessel. As the flow tapers off heat transfer at the vessel wall cools the side position but the center Tc remains at about 310K illustrating the very slow trend to full thermal equilibration. In fact the center Tc does not reach thermal equilibrium until about 60 s has elapsed (not shown).

The characteristics for the supply are simpler as is the flow within the vessel, with the side Tc remaining warmer than the center at all times as it is more rapidly affected by heat transfer from the wall.

The low pressure blowdown (360 psi- 200 psi) does not provide any useful data on the behavior of the receiver as it only changes a very small amount. The supply results are presented in Figures 14 and 15.



**Figure 14. 13L receiver and supply pressures**

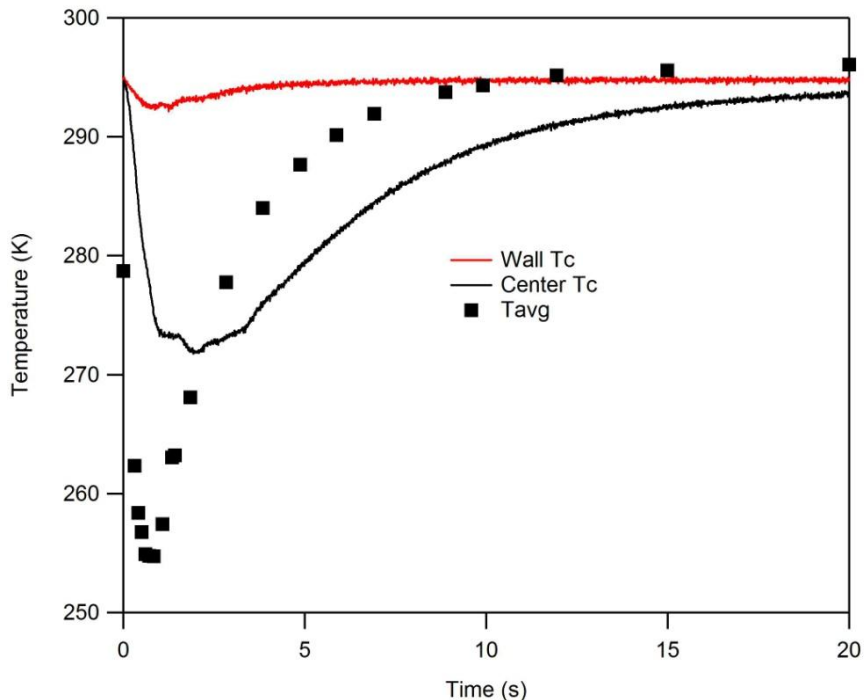


**Figure 15. Supply thermocouples and TPVT Tavg**

### 3.1.2. Error analysis

This experiment is unique in several ways. It represents the first set of measurements and it was not fully appreciated at the time what precision was needed for some of the procedures to obtain a good mass balance. In the instance of the 200-13000 experiment, the 13000 cc vessel was equipped with a 500 psi pressure transducer yet the maximum pressure in the experiment in the large receiver was only 82 psia. Thus, the pressure error could be as much as 0.35% of 500 psia or 1.75 psia or 2.1%. Compounding this with an error on the supply fill of as much as 0.5 % suggests that the mass balance error could be substantial. The observed maximum mass balance error of 2.6% when the gas was fully transferred to the receiver can be interpreted as mostly stemming from using the 500 psi transducer on the low end of its full scale range. The mass error associated with each data point is presented in Figure 16. We note that the first two points at early time were recorded several weeks before the rest of the data and thus drifts and other transients associated with the instrumentation probably cause these data to appear deviated from the bulk of the data. In addition, the receiver pressure transducer was unusually noisy (a condition later resolved). In fact the pressure measurements in the receiver for the first two early time data have signal-to-noise ratios not much more than 2.

The mass balance results for the low pressure (360 psia) 13L receiver experiment are not especially relevant given that only 3% of the gas at the start of the test is in the supply. The observed mass balance error was  $< 0.3\%$  and originates mostly because of thermocouple differences between the supply and the receiver.

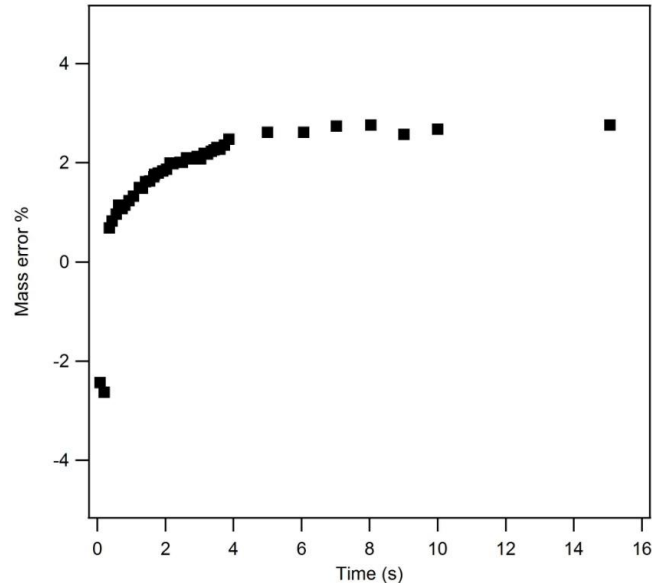


**Figure 16. Mass balance for the 6000 psia blowdown into the 13000 cc vessel**

### 3.2. 700 cc receiver

The 200 cc-700 cc configuration was used for three experiments with starting pressures of 300 psi, 3000 psi, and 6000 psi. The data were collected at 0.001 s intervals.

#### 3.2.1. General characteristics

Figure 17 shows the transient pressures for the 3000 psi fill for an uninterrupted blowdown into the 700 cc receiver indicating that pressure equilibrium was reached at 2.5 s. Figure 18 shows the  $T_{avg}$  TPVT results of the receiver and supply. For this much smaller receiver thermal equilibrium is achieved after about 30 s.

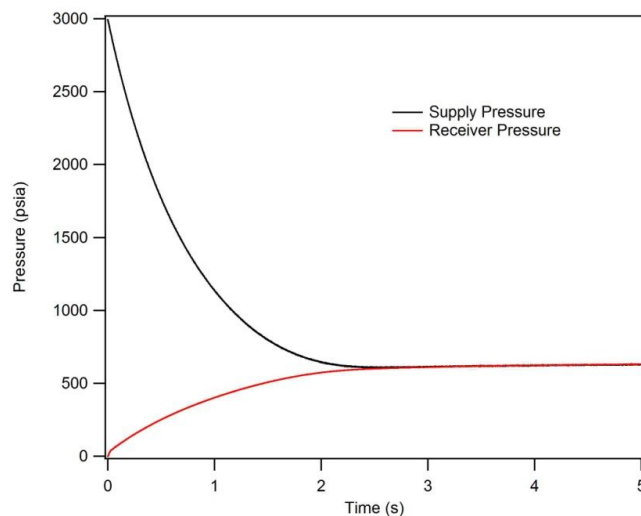


**Figure 17. Pressure traces for the 3000 psi blowdown into the 700cc receiver**

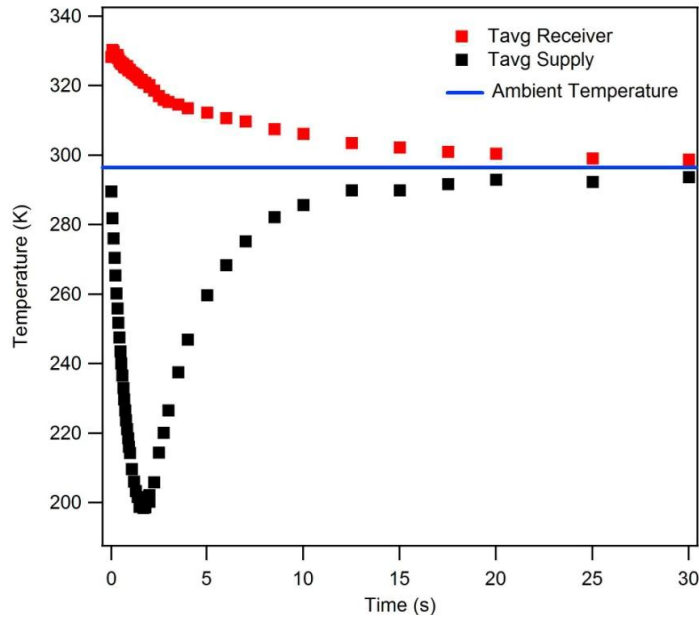


**Figure 18. TPVT Tavg for the 3000 psi 700 cc receiver blowdown**

### 3.2.2. Mass balance

Mass balances shown in Figure 19 in the 700 cc receiver experimental set are better than for the 13000 cc receiver. Error probably stems for the same source as discussed above. However, because the pressure transducers for the receiver were better sized than for the 13000 cc data in that the final receiver pressure is closer to the full scale output of the gauge, the mass balance errors are less.

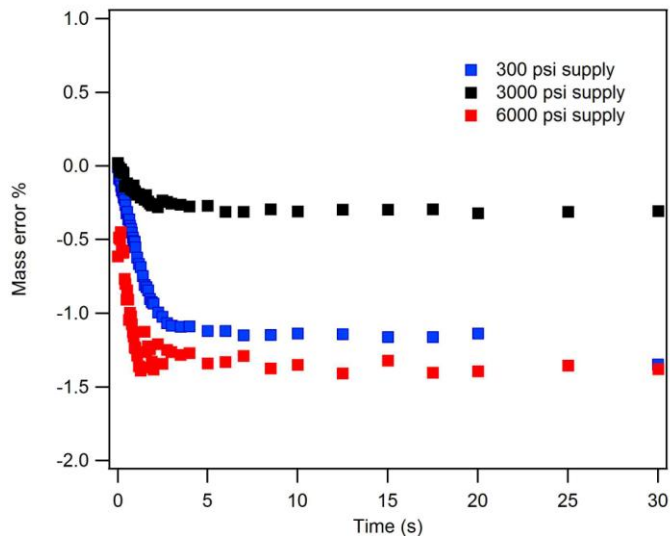


**Figure 19. Mass balances error for the three 700 cc receiver experiments**

### 3.3. 90 cc receiver

#### 3.3.1. General characteristics

Two experiments were conducted using a small 90 cc receiver: one at 3000 psi and another at 6000 psi. These experiments provide data that examines the receiver heat transfer characteristics at pressures as high as 4000 psi. Thus the combination of the three 700 cc receiver experiments and the two 90 cc experiments explore the nature of the heat transfer over a range of final gas densities in the receiver.

Figure 20 shows the results of the uninterrupted transfer from 6000 psi into the 90 cc receiver. Close examination of the traces show that the supply and receiver pressure transducers differ by approximately 42 psi when the two vessels are at pressure equilibrium near 3900 psia. In this test both transducer were 10000 psi FS gages, illustrating the inherent error of nearly 0.4% between them. Figure 21 shows the results for the supply and receiver thermocouples combined with the  $T_{avg}$  data for the TPVT measurements. The results for the 3000 psi supply experiment are similar to those presented in these figures.

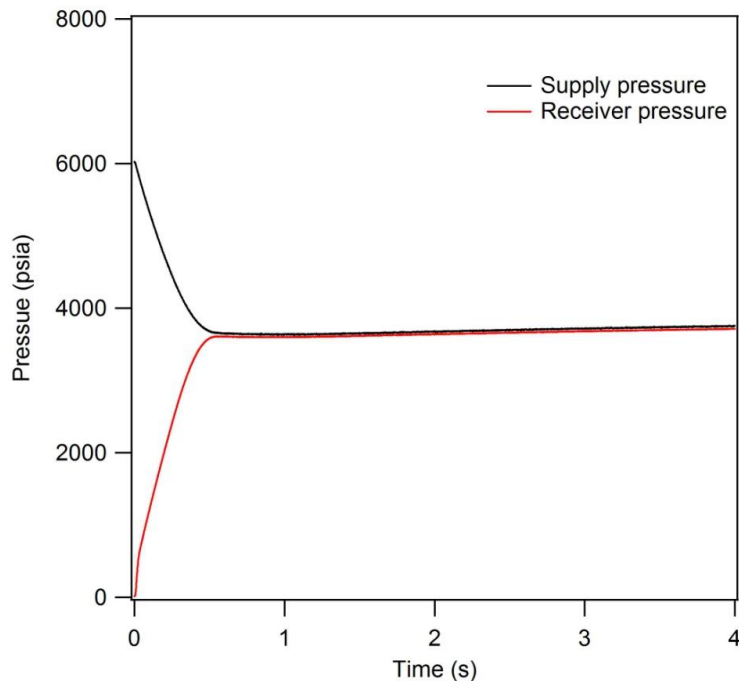
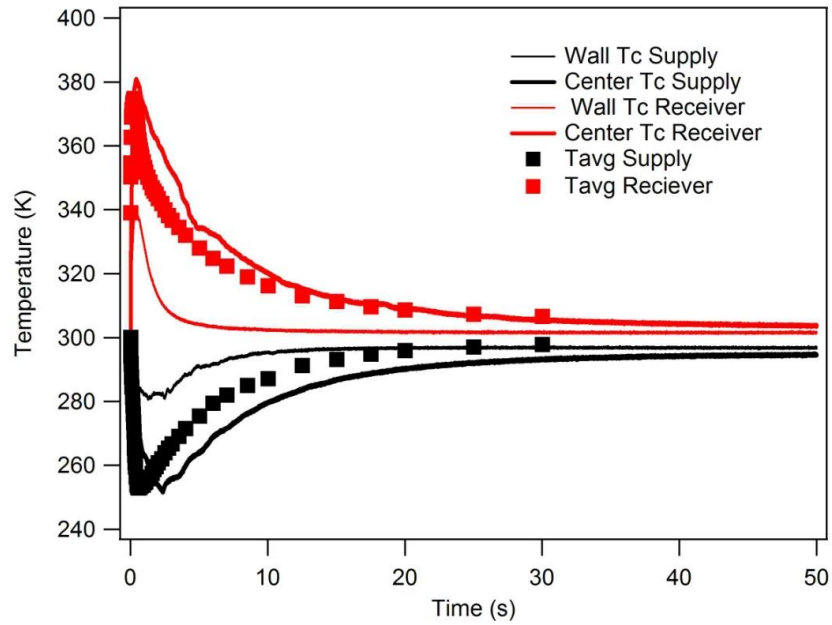


Figure 20. Pressure records for the 6000 psi blowdown into the 90 cc receiver



**Figure 21. Comparison of the TPVT Tavg temperatures and the internal thermocouples for the 6000 psi blowdown into the 90 cc receiver**

### 3.3.2. Mass balance

Mass balances in the experimental set, Figure 22, are better than for the 13000 cc receiver and similar to those obtained in the 700 cc experiments. Note that the approximate 0.4% mass balance error is on par with the 0.4% differential in the pressure transducers at equilibrium for the 6000 psi data.

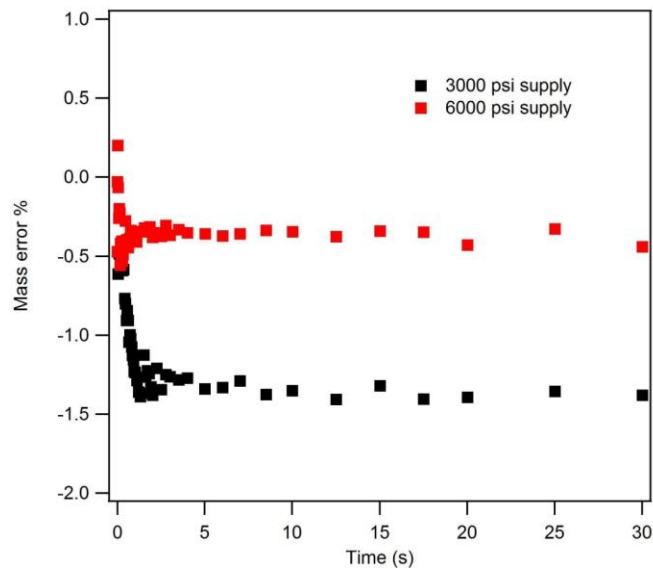


**Figure 22. 90 cc receiver mass error**

## 4. COMPARISON WITH NETFLOW

The primary motivation behind the previously described TPVT experiments was to obtain high quality data sets that could be used to validate and improve Sandia gas transfer models. Historically these models have been zero-dimensional and one-dimensional transient network flow models. In such models reservoir and receiver volumes are modeled using single control volumes and the tubing that connects these volumes is modeled using a series or string of control volumes. Solving the tube flow problem in a network flow modeling code is equivalent to solving the one-dimensional transient compressible flow conservation equations. For high speed compressible flow with large pressure differences between vessels, network flow codes must be able to identify locations where flow choking occurs and properly limit flow velocity to the sonic value.

Sandia's first network flow code dedicated to the solution of gas transfer problems was TOPAZ (Transient One-dimensional Pipe flow AnalyZer). TOPAZ has been extensively documented (see *e.g.* [6-10]). TOPAZ has been recently replaced by NETFLOW (see *e.g.* [11,12]) which utilizes an improved stiff differential-algebraic equation solver DASKR [15] for the solution of high speed compressible network flows.

Since the solution of the compressible network flow equations is restricted to zero or one dimension, correlations must be used to account for multidimensional effects. For example, frictional pressure-drop in tubing, an inherently multi-dimensional effect, is modeled using a quasi-steady correlation such as the one first proposed by Moody [16]. Similarly, multi-dimensional heat transfer effects in tube flow are modeled using a quasi-steady heat transfer correlation (see, *e.g.* Dittus and Boelter [17]).

Correlations must also be used to describe the multi-dimensional, transient effects of heat transfer in vessels. Unfortunately, existing correlations are very limited which is why network flow models that accurately predict transfer times (times to pressure equilibrium) often over predict or under predict transient vessel temperatures and hence masses delivered.

In this section we will compare NETFLOW predictions for vessel temperatures to those measured in the seven previously described transient PVT experiments. These predictions were made using the "default" NETFLOW vessel heat transfer correlations. The correlations have not been altered to provide better agreement with the measurements. In a follow-on document [18], Part II of this report, we will discuss improvements and limitations in the correlations and more directly address the nature of vessel heat transfer in supply vessels and receivers. We will also provide more detailed comparisons between NETFLOW predictions and the transient PVT experiments including comparisons of both pressure and temperature.

### 4.1 Heat transfer correlations

Detailed descriptions of the NETFLOW default heat transfer correlations are provided in Reference [19]. The reference also describes how the correlations are used in conjunction with the vessel energy equation to compute the mass averaged vessel temperature. This is the

temperature measured in the TPVT experiments. For the convenience of the reader, the default NETFLOW heat transfer correlations will be briefly summarized here.

Surprisingly little research has been done to characterize the heat transfer associated with the filling and evacuation of gases from vessels. Means [3] and Means and Ulrich [4] conducted a series of experiments to develop heat transfer correlations for tank filling and evacuation. Their correlations depend on the location of the gas entrance and exit with respect to gravity, the shape of the tank, and whether or not the flow is choked at the inlet. Means and Ulrich developed correlations to describe various modes of heat transfer. The default NETFLOW heat transfer correlation for receiver forced convection heat transfer is based on the functional forms suggested by Means and Ulrich. For the active part of the vessel fill in which gas is injected into the vessel, Means and Ulrich have shown that the following functional form seems to represent their data:

$$\text{Nu} = a \left[ \text{Re}_D \text{Pr} \left( \frac{d}{D} \right)^2 \right]^b \quad (6)$$

where the Nusselt number, Nu is given by

$$\text{Nu} = \frac{hD}{k} \quad (7)$$

the Reynolds number,  $\text{Re}_D$  is given by

$$\text{Re}_D = \frac{\rho_i v_i D}{\mu} = \frac{\dot{m}D}{A_i \mu} \quad (8)$$

and the Prandtl number, Pr is given by

$$\text{Pr} = \frac{C_p \mu}{k} . \quad (9)$$

and  $h$  is the heat transfer coefficient in Newton's law of cooling,  $D$  is the effective spherical diameter of the tank,  $d$  is the diameter of the inlet,  $k$  is the vessel gas thermal conductivity,  $\mu$  is the vessel gas dynamic viscosity,  $\rho_i$  is the gas density at the inlet,  $v_i$  is the inlet velocity,  $\dot{m}$  is the inlet mass flow rate,  $A_i$  is the inlet flow area and  $C_p$  is the vessel gas specific heat at constant pressure.

It should be pointed out that the Means and Ulrich correlation for forced convection was developed from measurements in which the inlet vessel flow was choked with properties that were constant in time. For Sandia applications, receiver inlet flow chokes and unchokes over time and properties vary considerably. Means and Ulrich used the constants 22 and 0.632 for  $a$  and  $b$  respectively. In NETFLOW the default value of the constant  $a$  was changed to 3.6.

Means and Ulrich suggested a free convection heat transfer correlation for the period of time after injection. Their free convection correlation takes the form

$$\text{Nu} = c\text{Ra}^n \quad (10)$$

where Ra is the Rayleigh number (defined below). The constants  $c$  and  $n$  depend on whether the flow is laminar or turbulent. For laminar flow ( $\text{Ra} < 1.24 \times 10^8$ )  $c$  and  $n$  take on values of 0.53 and 0.25 respectively. For turbulent flow ( $\text{Ra} > 1.24 \times 10^8$ )  $c$  and  $n$  take on values of 0.12 and 0.33 respectively. For gas transfer systems studied at Sandia these values were found to consistently under predict the heat transfer. As a result of experiments conducted at Sandia, Clark [2] suggested the following values for  $c$  and  $n$ :

$$\text{laminar flow (Ra} < 1.24 \times 10^8 \text{):} \quad c = 1.15, n = .22 \quad (11)$$

$$\text{turbulent flow (Ra} > 1.24 \times 10^8 \text{):} \quad c = 0.14, n = .333 \quad (12)$$

More recently these constants have been modified for NETFLOW. The values for  $c$  and  $n$  in the NETFLOW default free convection heat transfer correlation are given by:

$$\text{laminar flow (Ra} < 1.24 \times 10^8 \text{):} \quad c = 1.38, n = .22 \quad (13)$$

$$\text{turbulent flow (Ra} > 1.24 \times 10^8 \text{):} \quad c = 0.168, n = .333 \quad (14)$$

The Rayleigh number, Ra in the free convection correlation is given by

$$\text{Ra} = \text{Gr Pr} = \frac{g\beta(T - T_w)\rho^2 D^3 C_p \mu}{\mu^2 k} \quad (15)$$

where Gr is the Grashof number,  $g$  is the gravitational constant and  $\beta$ , the volume expansivity is given by

$$\beta = -\frac{1}{\rho} \left( \frac{\partial \rho}{\partial T} \right)_p = \frac{1 - B\rho}{T} \quad (16)$$

for an Abel-Noble gas. In the Rayleigh number definition  $T$  is the vessel mass averaged gas temperature,  $T_w$  is the wall temperature. The constant  $B$  in Eq. (16) is the Abel–Noble gas constant.

For vessels that act as supplies, interior flow velocities are negligible except for the small region just upstream of the exit. Hence the heat transfer is assumed to be governed solely by free convection. For vessels acting as receivers, multidimensional CFD calculations show (see e.g. Reference [18]) that during the initial injection the incoming jet stagnates against the opposite vessel wall and creates significant forced convection shear flows along the vessel wall. As pressure equilibrium is approached these flows diminish in strength and the dominant mode of

heat transfer transitions to free convection. For vessels acting as receivers NETFLOW assumes the following model for heat transfer:

$$\text{Nu} = \max(\text{Nu}_{forced}, \text{Nu}_{free}) \quad (17)$$

where  $\text{Nu}_{forced}$  is given by Equation (6) and  $\text{Nu}_{free}$  is given by Equation (5) and the constants given in Equations (13) and (14).

Once the vessel heat transfer Nusselt number is determined, NETFLOW computes the vessel heat transfer with Newton's law of cooling using the heat transfer coefficient

$$h = \frac{\text{Nu}k}{D} \quad (18)$$

where  $D$ , the characteristic dimension, is the diameter of an "equivalent" spherical vessel. For vessels that are not spherical,  $D$  is calculated from the tank volume,  $V$  using the following expression:

$$D = \left( \frac{6V}{\pi} \right)^{\frac{1}{3}} \quad (19)$$

## 4.2 Model-data comparisons

In the model-data comparisons that follow (Figures 23-29) all transfers were made from a 200 cc (nominal) supply volume. The receiver volume and the initial supply pressures were varied to capture a range of vessel heat transfer situations.

Figures 23-25 illustrate the influence of initial supply pressure level on the transfer between a 200 cc nominal supply and a 700 cc nominal receiver. Supply pressures for Figures 23, 24, and 25 were 300, 3000 and 6000 psi respectively (nominal values). Higher initial supply pressures result in larger transient temperature excursions for both the supply and the receiver. This expected and observed trend is well replicated by the NETFLOW models. Predicted temperature transients for the supply are in excellent agreement with the measurements. The timing and magnitude of the minimum supply temperature spike and the recovery back to ambient temperature are accurately reproduced by NETFLOW. Predictions for the receiver are more qualitative. With the current default receiver heat transfer model, the peak temperature in the receiver is consistently over predicted although the time required for the decay back to ambient temperature is in good agreement with the measurements at later times.

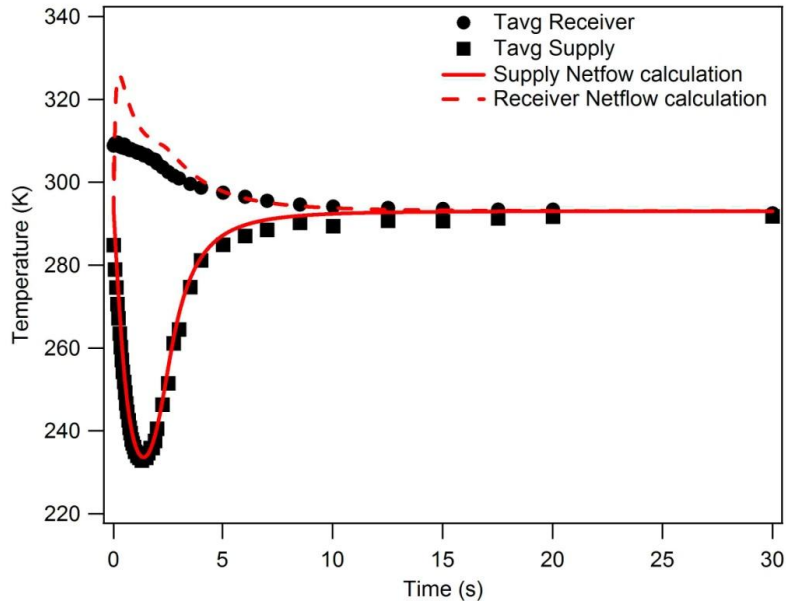


**Figure 23. Measured and predicted supply (200 cc) and receiver (700 cc) mass averaged temperatures. Initial supply pressure was 300 psi (nominal)**

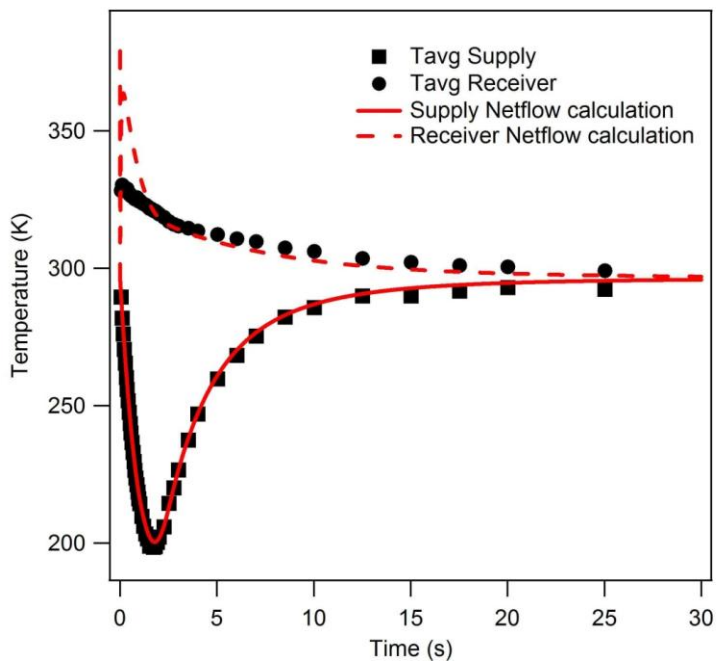


**Figure 24. Measured and predicted supply (200 cc) and receiver (700 cc) mass averaged temperatures. Initial supply pressure was 3000 psi (nominal)**

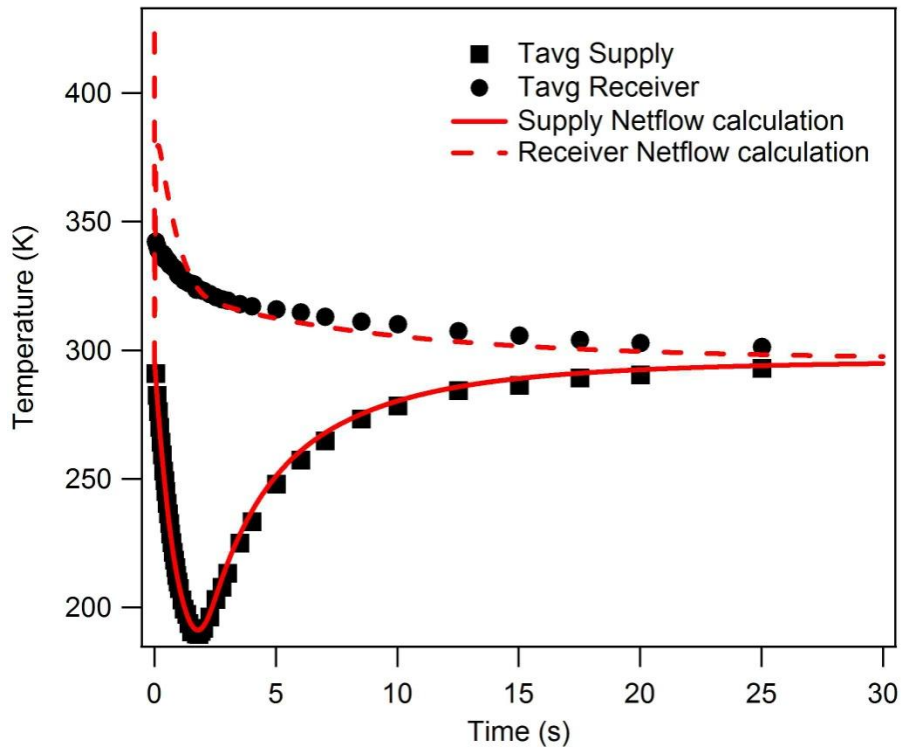


**Figure 25. Measured and predicted supply (200 cc) and receiver (700 cc) mass averaged temperatures. Initial supply pressure was 6000 psi (nominal)**

Figures 26 and 27 illustrate the influence of reducing the receiver size from a nominal 700cc to a nominal 90cc. Initial supply pressures for the comparisons in Figures 26 and 27 were 3000 and 6000 psi respectively. The influence of reduced receiver size is evident when Figure 24 is compared to Figure 26 (both 3000 psi nominal supply pressure) and Figure 27 is compared to Figure 25 (both 6000 psi nominal supply pressure). Although it is not evident from looking at temperature transients, reducing the receiver size from 700 to 90 cc reduces the transfer time to pressure equilibrium from approximately 2 seconds to 0.5 seconds. This is true for both the 3000 and 6000 psi supply. Reducing the receiver size reduces the pressure change in the supply and results in a corresponding smaller drop in the supply transient temperature. Conversely, reducing the receiver size increases the pressure change in the receiver resulting in a correspondingly higher transient temperature spike. This behavior is observed in the experiments and is predicted by the modeling. As was the case for the comparisons in Figures 23-25, the comparisons shown in Figures 26 and 27 show that the supply temperature transient is well replicated by the modeling while the receiver prediction is more qualitative with the early temperature spike being over predicted.

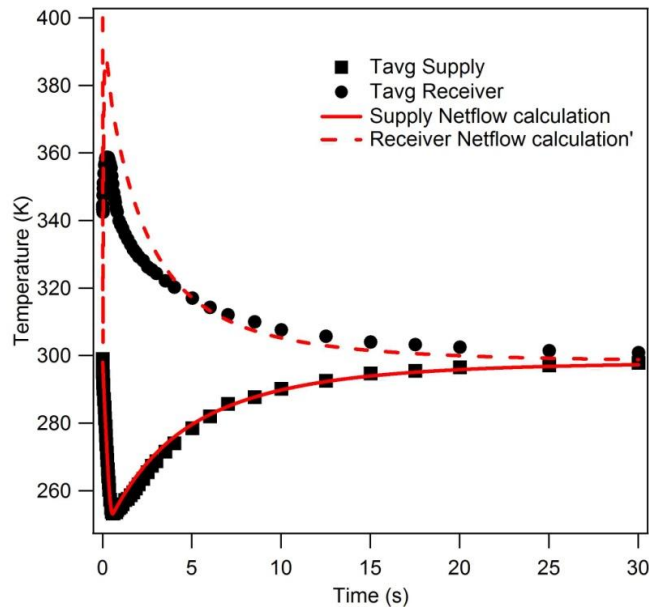


**Figure 26. Measured and predicted supply (200 cc) and receiver (90 cc) mass averaged temperatures. Initial supply pressure was 3000 psi (nominal)**

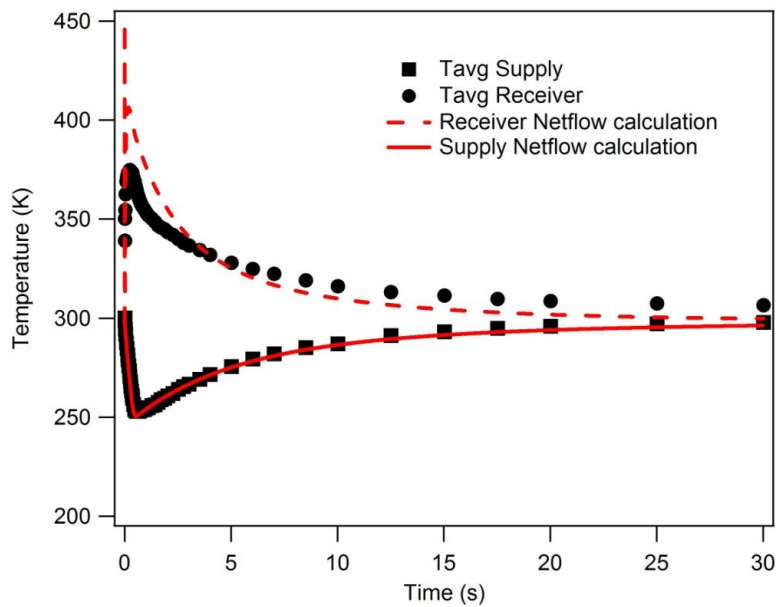


**Figure 27. Measured and predicted supply (200 cc) and receiver (90 cc) mass averaged temperatures. Initial supply pressure was 6000 psi (nominal)**

Figures 28 and 29 illustrate the influence of using a large receiver volume, in this case 13 liters (13,000 cc). Figure 28 shows temperature transients for a high pressure ratio transfer (6000:14.7) in which a large portion of the transfer takes place with choked flow at the orifice. Choked flow was also present in all the comparisons previously discussed (*i.e.* Figures 23-27). The model-data comparison in Figure 29 shows temperature transients for a low pressure ratio transfer (350:200) in which no choking occurs. (For choking to occur in this test the initial supply pressure would have to be increased to at least 410 psi while keeping the initial receiver pressure at 200 psi.) . In each comparison the measured supply temperature transient is well predicted by the model. Once again the spike in receiver temperature is over predicted by the model in the high pressure ratio transfer. The increase in receiver temperature for the low pressure ratio test (Figure 29) is quite small and scatter in the data makes it difficult to make a judgment on the accuracy of the prediction. The small temperature rise in the receiver is due to the fact that a relatively small amount of gas was added to the receiver during the transfer.

The tests shown in Figures 28 and 29 were among some of the first transient PVT tests conducted. For the test depicted in Figure 28, uncertainty exists in identifying the representative starting supply and receiver temperatures. Not all transient PVT tests were started from the same temperature (supply  $T = 30 \pm 1.7$  °C) and as previously stated the precision of the pressure measurement is in question. This explains why the predicted temperatures actually cross each other at 12 seconds. The model assumed that the starting receiver temperature was several degrees lower than the supply temperature. The receiver temperature data scatter in Figure 29 is also attributable to the fact that this was an early test in which the experimental technique was being developed and perfected. Despite the experimental uncertainties, these two data sets are extremely valuable since they reinforce our understanding of vessel heat transfer.

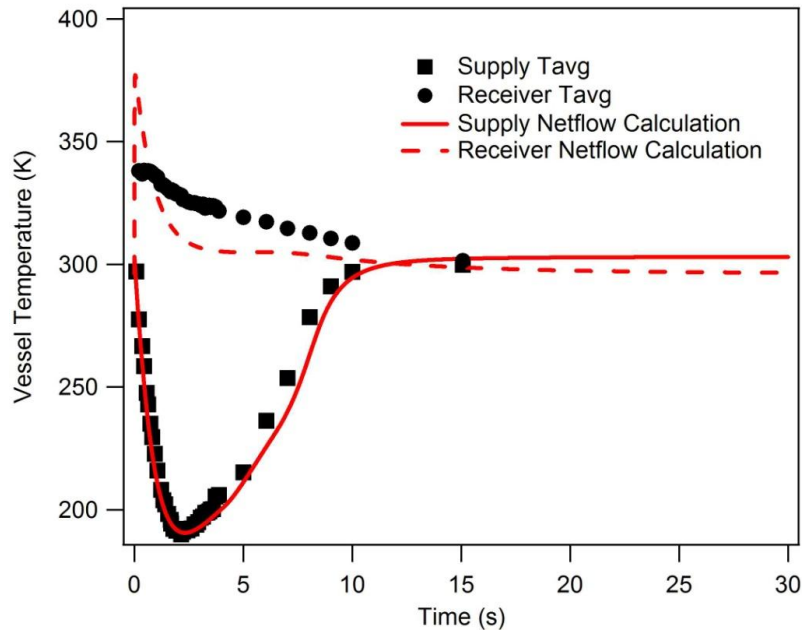


**Figure 28. Measured and predicted supply (200 cc) and receiver (13 liter) mass averaged temperatures. Initial supply pressure was 6000 psi (nominal)**

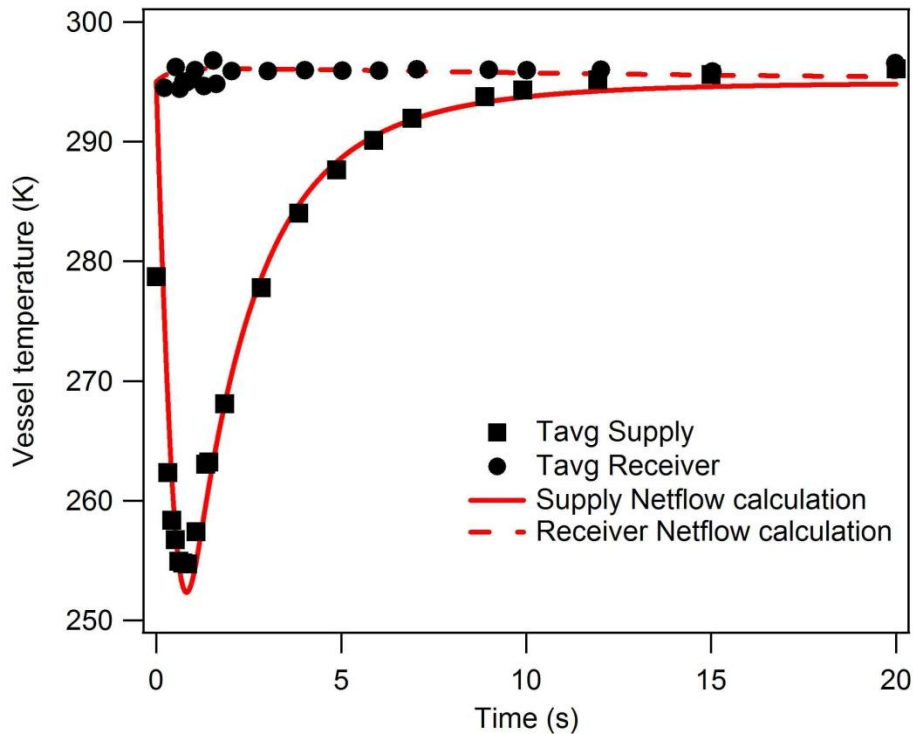


**Figure 29. Measured and predicted supply (200 cc) and receiver (13 liter) mass averaged temperatures. Initial supply and receiver pressures: 360 and 200 psia respectively**

### 4.3 Modeling summary

The model-data comparisons discussed in this chapter show that for monotonic supply blowdowns the nominal vessel heat transfer model is quite accurate. This model is based on the assumption that heat transfer in the supply is governed by free convection. The leading coefficients in the laminar and turbulent free convection heat transfer correlations used in NETFLOW are approximately 20% greater than those previously reported by others ( see *e.g.* [2,3]).

The default NETFLOW heat transfer model for receivers needs more work. Peak temperature spikes are consistently over predicted although the temperature decay back to ambient is fairly well predicted by the model. The receiver model is based on two modes of heat transfer, a forced convection mode that dominates during the early portion of the injection when the flow is pressure driven and a free convection mode identical to that used for the supply.

The transient PVT data presented in this document are currently being used to improve the NETFLOW receiver heat transfer model. These improvements and a more detailed discussion of modeling and the nature of vessel heat transfer are contained in the follow-on document [18].



## 5. CONCLUSION

A series of high pressure vessel-to-vessel gas transfers were conducted using Transient PVT methodology to determine dynamic mass-averaged vessel temperatures and to provide data sets to validate CFD and network flow models. Models developed for gas transfer must account for vessel heat transfer in order to accurately predict masses transferred. To date, the modeling approach has been to use correlations established several decades ago that relate the spatially averaged Nusselt number to flow parameters and some geometrical factors via relatively simple expressions.

The experiments consisted of different pressurized fill quantities for a single 200 cc source vessel rapidly blowing down into three different receiver vessels ranging in volume. Specifically, the receiver volumes were 90 cc, 700 cc, and 13000 cc nominally. Several initial pressures were examined. The transient PVT data were reduced to quantify the mass transferred as a function of time. In turn, the transient mass averaged temperature,  $T_{avg}$ , for both the receiver and the 200 cc supply vessel was calculated from the transient mass, transient pressure, known volumes, and a real-gas EOS. The results are compared with those calculated from NETFLOW using baseline heat transfer correlations.

The comparisons show that the simple heat transfer correlations for the supply vessel in which the internal flow velocities are very small appears work very well. The transient  $T_{avg}$  for the supply was well represented in all cases over the entire transfer time including the thermal equilibration time that occurs subsequent to the system achieving pressure equilibrium. However, the results show that the correlation on the receiver side of the event do not properly capture the early time heat transfer from the gas. In all cases, the model tended to over predict  $T_{avg}$  and therefore did not capture the highly transient and spatially nonuniform nature of the receiver heat transfer at early times in the fill.

This work has been conducted in conjunction with a 3-Dimensional Navier-Stokes modeling project using the ASC code FUEGO. Results from that modeling effort and improvements to the NETFLOW heat transfer correlations will be presented in a subsequent report titled “Comparisons of High Pressure Transient PVT Measurements and Model Predictions – Part II”.



## 6. REFERENCES

1. S. C. Johnston. *A Characterization of Unsteady Gas Discharge from a Vessel*, Sandia National Laboratories SAND83-8226, July 1983.
2. G. L. Clark, *A Zero-Dimensional Model of Compressible Gas Flow in Networks of Pressure Vessels – Program TRIC*, SAND83-8226, Sandia National Laboratories, Livermore, CA, July 1983.
3. J. D. Means, *Transient Convection Heat Transfer in Closed Containers During and After Injection*, Ph.D Thesis, Brigham Young University 1973.
4. J. D. Means and R. D. Ulrich, *Transient Convective Heat Transfer During and After Gas Injection into Containers* Journal of Heat Transfer, ASME, p.282 May 1975.
5. B. A. Meyer, Personal communication (1983).
6. W. S. Winters, *TOPAZ-A Computer Code for Modeling Heat Transfer and Fluid Flow in Arbitrary Networks of Pipes, Flow Branches and Vessel*, SAND83-8253, Sandia National Laboratories, Livermore, CA, January 1984.
7. W. S. Winters, *TOPAZ-The Transient One-Dimensional Pipe Flow Analyzer: User's Manual*, Sandia Technical Report SAND85-8215, Sandia National Laboratories, Livermore, CA, July 1985.
8. W. S. Winters, *TOPAZ-The Transient One-Dimensional Pipe Flow Analyzer: Code Validation and Sample Problems*, Sandia Technical Report SAND85-8236, Sandia National Laboratories, Livermore, CA, October 1985.
9. W. S. Winters, *TOPAZ-The Transient One-Dimensional Pipe Flow Analyzer: Equations and Numerics*, Sandia Technical Report SAND85-8248, Sandia National Laboratories, Livermore, CA, December 1985.
10. W. S. Winters, *TOPAZ-The Transient One-Dimensional Pipe Flow Analyzer: An Update on Code Improvements and Increased Capabilities*, Sandia Technical Report SAND87-8225, Sandia National Laboratories, Livermore, CA, September 1987.
11. W. S. Winters, *A New Approach to Modeling Fluid/Gas Flows in Networks*, Sandia Technical Report, SAND2001-8422, Sandia National Laboratories, Livermore, CA, July 2001.
12. W. S. Winters, *Implementation and Validation of the NETFLOW Porous Media Model* Sandia Technical Report, SAND2009-6838, Sandia National Laboratories, Livermore, CA, December 2009.

13. E.E. Fischer and A.D. Shugard, *Characterization of New Precision Volume Measurement System*, Sandia National Laboratories, Livermore, CA, November 2004
14. S. C. Keeton, Classified Sandia Report, SAND76-8240, Sandia National Laboratories, Livermore, California, July 1976.
15. L. R. Petzold, P. N. Brown, A. C. Hindmarsh, and C. W. Ulrich, *DDASKR – Differential Algebraic Solver Software*, Center for Computational Science & Engineering, L-316, Lawrence Livermore National Laboratory, P.O. Box 808, a private communication with L. R. Petzold.
16. L. F. Moody, *Friction Factors for Pipe Flow*, *Trans. ASME*, volume 66, No. 8 p. 671, 1944.
17. F. W. Dittus and L. M. K Boelter, *University of California (Berkeley) Pub. Eng. Volume 2*, p. 443, 1930.
18. W. S. Winters, G. H. Evans, S. F. Rice, N. J. Paradiso and T. G. Felver, *Comparison of High Pressure Transient PVT Measurements and Model Predictions – Part II*, Sandia Technical Report, SAND2010-XXXX, Sandia National Laboratories, Livermore, CA, in preparation.
19. W.S. Winters, *Modeling Vessel Fillup and Blowdown*, Sandia Technical Report, SAND2009-0100, Sandia national Laboratories, Livermore, CA, January, 2009.

## DISTRIBUTION

1	MS9001	C. D. Moen	08005 (electronic copy)
1	MS9035	P. A. Spence	08224 (electronic copy)
1	MS9035	C. A. LaJeunesse	08224 (electronic copy)
1	MS9035	A. H. Leung	08224 (electronic copy)
1	MS9035	B. E. Oden	08224 (electronic copy)
1	MS9035	N. J. Paradiso	08224
2	MS9035	S. F. Rice	08224
1	MS9035	B. Markel	08224 (electronic copy)
1	MS9054	R. W. Carling	08300 (electronic copy)
1	MS9153	M. F. Hardwick	08220 (electronic copy)
1	MS9154	J. L. Bowie	08237 (electronic copy)
1	MS9154	R. A. Van Cleave	08237 (electronic copy)
1	MS9154	J. P. Chan	08244 (electronic copy)
1	MS9154	C. W. Pretzel	08244 (electronic copy)
1	MS9161	S. K. Griffiths	08300 (electronic copy)
1	MS9161	A. E. Pontau	08360 (electronic copy)
1	MS9161	R. H. Nilson	08365 (electronic copy)
1	MS9292	M. P. Kanouff	08365 (electronic copy)
1	MS9409	Ralph Greif	08365 (electronic copy)
1	MS9409	N. R. Fornaciari	08365 (electronic copy)
1	MS9409	D. E. Dedrick	08365 (electronic copy)
1	MS9409	S. C. James	08365 (electronic copy)
2	MS9409	G. H. Evans	08365
1	MS9409	W. G. Houf	08365 (electronic copy)
1	MS9409	J. A. Templeton	08365 (electronic copy)
1	MS9409	G. J. Wagner	08365 (electronic copy)
2	MS9409	W. S. Winters	08365
1	MS9661	A. D. Shugard	08224 (electronic copy)
1	MS9661	S. Stieper	08224 (electronic copy)
1	MS9661	L. Thai	08224 (electronic copy)
1	MS9661	P. Van Blarigan	08224 (electronic copy)
1	MS9661	T. G. Felver	08224
1	MS0899	Technical Library	09536 (electronic copy)
2	MS9960	Technical Library-CA	08944





